Article

Electronic Band Gap Tuning and Calculations of Mechanical Strength and Deformation Potential by Applying Uniaxial Strain on MX$_2$ (M = Cr, Mo, W and X = S, Se) Monolayers and Nanoribbons

Anjna Devi,* Narender Kumar, Abu Thakur, Arun Kumar, Amarjeet Singh, and P. Kumar Ahluwalia
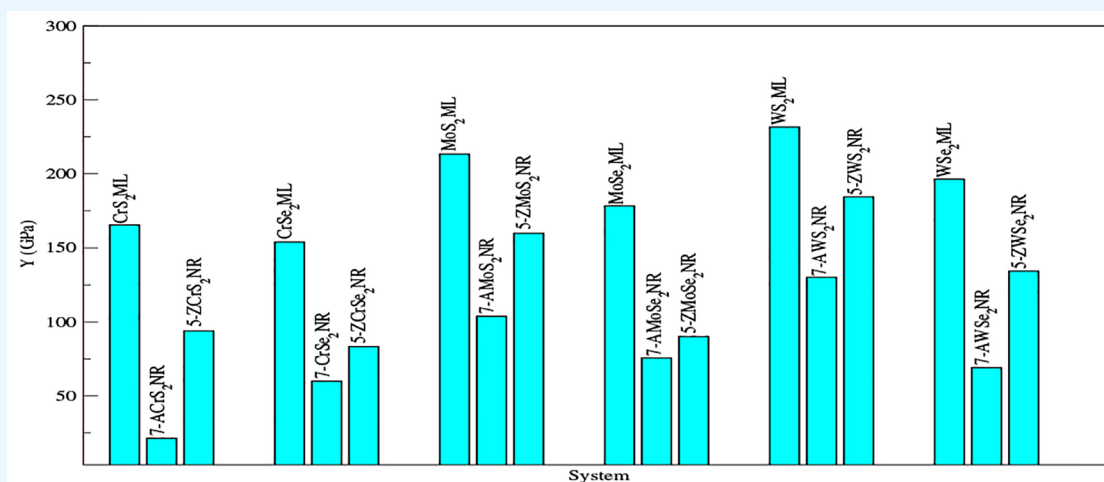
Read Online

ACCESS | Metrics & More | Article Recommendations | SI Supporting Information

ABSTRACT: Two-dimensional (2D) transition-metal dichalcogenides (TMDs) are new crystalline materials with exotic electronic, mechanical, and optical properties. Due to their inherent exceptional mechanical strength, these 2D materials provide us the best platform for strain engineering. In this study, we have performed first-principles calculations to study the effect of uniaxial strains on the electronic, magnetic, and mechanical properties of transition-metal dichalcogenides (TMDs) MX$_2$ (where M = Cr, Mo, W and X = S, Se), monolayers (2D), and armchair and zigzag nanoribbons (1D). For the mechanical strength, we determined the tensile strength (σ) and Young's modulus (Y) and observed that σ and Y are higher in monolayers (most in WS$_2$ML) as compared to nanoribbons where monolayers resist tension up to 25−28% strain while nanoribbons (armchair and zigzag) can be only up to 5−10%. Deformation potential (Δ_p) in the linear regime near the equilibrium position ($\epsilon < 2\%$) has also been calculated, and its effect on monolayers is observed less as compared to nanoribbons. In addition, unstrained nonmagnetic monolayers are direct band gap semiconductors (D) which changed to indirect band gap semiconductors (I) with the application of strain. Ferromagnetic states of metallic zigzag nanoribbons (including up spin channel of 7-CrS$_2$NR and 7-CrSe$_2$NR) are greatly affected by strain and show half-metal-like behavior in different strain range. The magnetic moment (μ) that is predominantly observed in zigzag nanoribbons is 2 times higher than that of other nanoribbons. This magnetism in nanoribbons is mostly caused by transition-metal atoms (M = Cr, Mo, W). Thus, our study suggests that strain engineering is the best approach to modify or control the structural, electronic, magnetic, and mechanical properties of the TMD monolayer and nanoribbons which, therefore, open their potential applications in spintronics, photovoltaic cells, and tunneling field-effect transistors.

■ INTRODUCTION

Over the past decade, two-dimensional (2D) materials have attracted great research interest due to their novel electronic and mechanical properties[1−7] and have been found to be potential candidates for future piezoelectric devices,[1,8] flexible electronics,[9] strain sensors[10] and nanoelectro-mechanical devices (NEMD).[11] The era of 2D materials started with the invention of graphene in 2004.[12,13] Graphene has an atomically thin honeycomb structured layer of carbon atoms with sp^2

hybridization,[14] high electron mobility,[15] thermal conductivity,[16] and exceptional mechanical properties.[17−20] Motivated
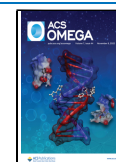
Table 1. Unstrained Lattice Constant (a_0), Unstrained Energy Band Gap (E_{g0}), Deformation Potential (Δ_p), Percentage of Tensile Strain (ϵ), Tensile Strength (σ^m), and Young's Modulus (Y) for the Studied MX$_2$MLs

system	a_0 (Å)	E_{g0} (eV)	Δ_p (eV)	tensile strain (%)		tensile strength (GPa)		Y_{xx} (GPa)	Y_{yy} (GPa)
				(ϵ_{xx})	(ϵ_{yy})	(σ^m_{xx})	(σ^m_{yy})		
CrS$_2$ML	3.072[a]	0.970 (D)[a]	−7.4	25	25	23.68	23.18	165.5	164.2
CrSe$_2$ML	3.235[a]	0.789 (D)[a]	−1.9	27	27	20.47	20.47	154.5	153.9
MoS$_2$ML	3.207[a]	1.626 (D)[a]	−11.4	26	25	25.40	25.43	213.4	216.4
			−12.0[g]			16−30[c], 22 ± 4[e]		217.6[d], 197[f]	
MoSe$_2$ML	3.340[a]	1.46 (D)[a]	−4.5	28	25	22.48	22.49	178.4	178.2
			−4.5[g]					171.4[d]	
WS$_2$ML	3.214[a]	1.83 (D)[a]	−12.9	28	27	28.06	27.98	231.5	231.6
	3.24[b]	1.73 (D)[b]						218.8[d]	
WSe$_2$ML	3.345[a]	1.582 (D)[a]	−5.9	28	28	24.52	24.53	196.5	196.3
								201.5[d]	

[a]Reference 40 (earlier work). [b]Reference 63. [c]Reference 64. [d]Reference 65. [e]Reference 10. [f]Reference 66. [g]Reference 67.

Table 2. Unstrained Lattice Constant (a_0), Unstrained Energy Band Gap (E_{g0}), Deformation Potential (Δ_p), Magnetic Moment (μ_0), Conductance (G), Percentage of Tensile Strain (ϵ_{xx} for Zigzag NRs and ϵ_{yy} for Armchair NRs), Tensile Strength (σ_{xx} for Zigzag NRs and σ_{yy} for Armchair NRs), and Young's Modulus (Y_{xx} for Zigzag NRs and Y_{yy} for Armchair NRs) for the Studied MX$_2$NRs

system	a_0 (Å)	E_{g0} (eV)	Δ_p (eV)	μ_0 ($\mu_{B/basis}$)	G (G_0)	$\epsilon_{xx/yy}$ (%)	$\sigma^m_{xx/yy}$ (GPa)	$Y_{xx/yy}$ (GPa)
7-ACrS$_2$NR	5.369[a]	0.132 (D) ↑[a]	−3.8	0.571[a]	−	10	4.84	21.5
		0.688 (I) ↓[a]	−2.6		−			
5-ZCrS$_2$NR	3.169[a]	−	−	0.800[a]	2 ↑[a]	6	4.86	93.9
		0.626 (I) ↓[a]	+6.4		−			
7-ACrSe$_2$NR	6.079[a]	0.322 (D) ↑[a]	+0.7	0.571[a]	−	10	5.71	60.0
		0.543 (D) ↓[a]	−1.4		−			
5-ZCrSe$_2$NR	3.393[a]	−	−	0.606[a]	1 ↑[a]	10	5.86	83.3
		−	−		2 ↓[a]			
7-AMoS$_2$NR	5.510[a]	0.396 (I)[a]	−0.2	0.000[a]	−	10	7.96	103.4 (136)[b]
5-ZMoS$_2$NR	3.170[a]	−	−	0.366[a]	3 ↑[a]	9	8.47	159.9
		−	−		3 ↓[a]			
7-AMoSe$_2$NR	5.752[a]	0.22 (I)[a]	+1.1	0.000[a]	−	7	4.92	75.6
5-ZMoSe$_2$NR	3.311[a]	−	−	0.436[a]	4 ↑[a]	5	4.62	90.1
					7 ↓[a]			
7-AWS$_2$NR	5.520[a]	0.36 (D)[a]	+0.5	0.000[a]	−	8	7.98	130.2
5-ZWS$_2$NR	3.174[a]	−	−	0.364[a]	3 ↑[a]	8	9.79	184.5
					2 ↓[a]			
7-AWSe$_2$NR	5.687[a]	0.384 (I)[a]	+1.8	0.000[a]	−	7	4.83	69.1
5-ZWSe$_2$NR	3.316[a]	−	−	0.343[a]	3 ↑[a]	8	6.22	134.3
					2 ↓[a]			

[a]Reference 40 (earlier work). [b]Reference68.

by graphene, various other graphene-like 2D nanomaterials, such as the hexagonal-boron nitride,[21] silicene/germanene,[22,23] transition-metal dichalcogenides (TMDs),[24−27] phosphorene,[28] carbides and nitrides[29,30] and many more have been studied extensively.

Among various 2D nanomaterials, applications of TMDs in various fields such as electronics,[31] optoelectronics,[32,33] photonics,[34−36] sensors,[1,8−10,37] thermoelectrics,[38] catalysis,[39] etc. have shown great promise, which leads to development of new technologies. More than 40 different categories of various TMDs have been explored so far in which CrS$_2$, CrSe$_2$, MoS$_2$, MoSe$_2$, WS$_2$, and WSe$_2$ monolayers (MLs) are switched for applications in electronics.[6,24,40,41]

Also, in past years, researchers have found that one-dimensional (1D) nanostructures (i.e nanoribbons, nanotubes, nanoflakes, and nanowires) also show excellent properties due to quantum confinement, low dimensionality, and edge effects.[40,42−44] Hence, confining 2D nanostructures/mono-

layers to 1D nanoribbons of MX$_2$-layered materials further extends their applications in various fields.[45−47]

Strain-induced electronic band structure tuning is another way to further fine-tune the properties of TMDs which helps us design devices that are very helpful in the piezoelectric industry, flexible electronic devices, and NEMDs.[1,8−11] Because of the wide-range tunability of the energy band gap of TMDs via strain, they have been studied both experimentally[48,49] and theoretically.[32,33,37,50] Qi et al. have studied edge stresses in MoS$_2$ML.[51] Zhang et al. showed that the band gap of WX$_2$ (X = S, Se) increases with increasing strain.[52] The effect of tensile strains on the electronic properties of early TMD monolayers (TMDMLs) MX$_2$ (M = Sc, Ti, Zr, Hf, Ta, Cr; X = S, Se, and Te) was studied by Guo et al.[53] Strain engineering in single, bi-, and trilayer MoS$_2$, MoSe$_2$, WS$_2$, and WSe$_2$ was studied by Carrascoso et al.[54] Electronic and magnetic properties of MoS$_2$[55] and WS$_2$[56] nanoribbons could be controlled by applying strain, indicating

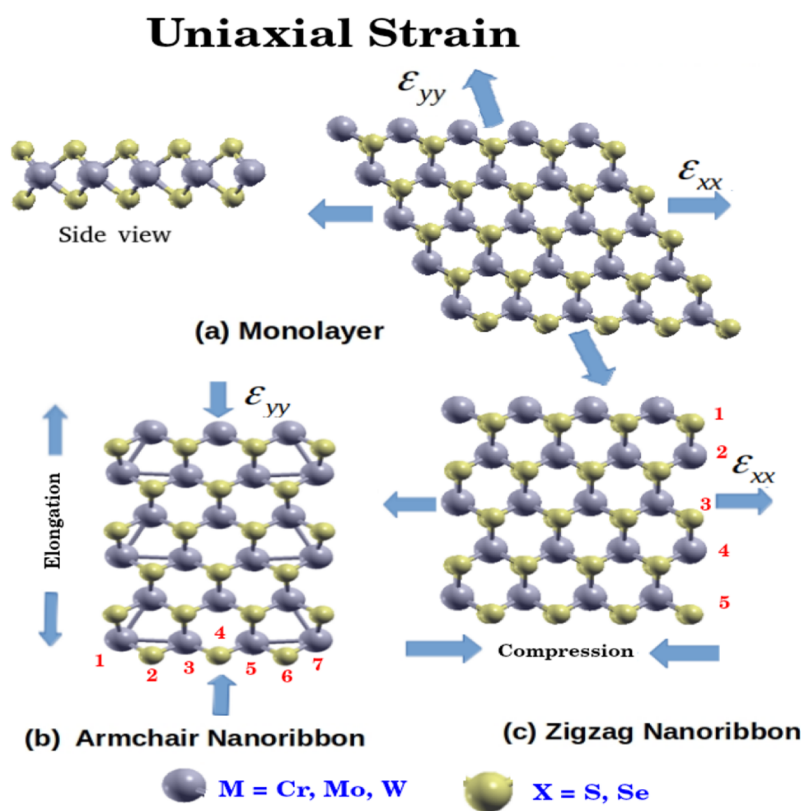**Figure 1.** Representative scheme of MX_2 (M = Cr, Mo, W and X = S, Se) with applied strain along its periodic axis: (a) MX_2 monolayers with elongative uniaxial strain (EUS) and compressive uniaxial strain (CUS) along the x-direction (ϵ_{xx}) and y-direction (ϵ_{yy}). (b) Armchair nanoribbons (AMX_2NR) with EUS and CUS along the y-direction (ϵ_{yy}). (c) Zigzag nanoribbons ZMX_2NR with EUS and CUS along the x-direction (ϵ_{xx}). Numbers 5 and 7 represent the ribbon width.

their potential applications to spintronics and photovoltaic cells.

To the best of our knowledge, no studies have been performed using uniaxial strain (US) on the spin-dependent mechanical properties of TMD nanoribbons and their comparison with the corresponding TMD monolayers. In addition to various available studies on TMD monolayers, we have systematically studied the effect of uniaxial strain on the electronic band structure of nanoribbons (both armchair and zigzag nanoribbons) and compare them with the corresponding monolayers.

METHODOLOGY

First-principles-based calculations for all MLs and NRs of TMDs were conducted using SIESTA (Spanish Initiative for Electronic Simulations with Thousands of Atoms).[57,58] Troullier−Martins norm conserving, relativistic pseudopotential, and the generalized gradient approximation (GGA) within the format of Perdew−Burke−Ernzehof (PBE)[59] was used for the exchange-correlation functional. Structures have been relaxed until each atom has forces less than 0.01 eV/Å. We have employed double-ζ polarization (DZP) basis sets with a confinement energy of 20 meV and 350 Ry mesh cutoff energy in all our simulations. $15 \times 15 \times 1$, $15 \times 1 \times 1$, and $1 \times 15 \times 1$ Monkhorst pack for 2D (monolayer of MX_2) and 1D (armchair and zigzag nanoribbons of MX_2) systems, respectively, have been used for Brillouin zone integration.[60] A vacuum of about 15 Å has been used to avoid interactions between periodic images. We have modeled a single-layered 2D sheet of all MX_2 (M = Cr, Mo, W, and X = S, Se) by taking

three atoms (one M and two X) per unit cell. The armchair and zigzag nanoribbons of all MX_2 are formed by cutting a MX_2 monolayer along different directions followed by 21 (7 M and 14 X atoms) and 15 (5 M and 10 X atoms) atoms per unit cell for modeling armchair and zigzag nanoribbons, respectively.

RESULTS AND DISCUSSION

To investigate the electronic and mechanical properties of unstrained (UTMD) and strained transition metal dichalcogenides (STMD), we first relaxed the atomic positions and lattice vectors to obtain the optimized geometry of each monolayer and nanoribbon of MX_2 (MX_2ML and MX_2NR). The relaxed configurations were obtained by minimizing the total energies of each systems. All the optimized lattice parameters for UTMD and STMD are listed in Table 1 and 2. We have compared our results with available results of MX_2MLs[52−54,61,62] and they are in good agreement with the available data. The unstrained band gap (E_{g0}) and lattice constant (a_0) of all monolayers and nanoribbons (armchair and zigzag) are computed and given in Tables 1 and 2. All unstrained monolayers (CrS_2, $CrSe_2$, MoS_2, $MoSe_2$, WS_2, and WSe_2) are direct band gap semiconductors. Armchair nanoribbons (unstrained) are both direct as well as indirect semiconductors while zigzag nanoribbons are metallic, and the results are in good agreement with previous DFT results and our earlier work.[40] The effect of strain on monolayers and nanoribbons explained below.

Strain Effect on Structural Properties. The crystal structure of the MX_2 monolayers and nanoribbons under
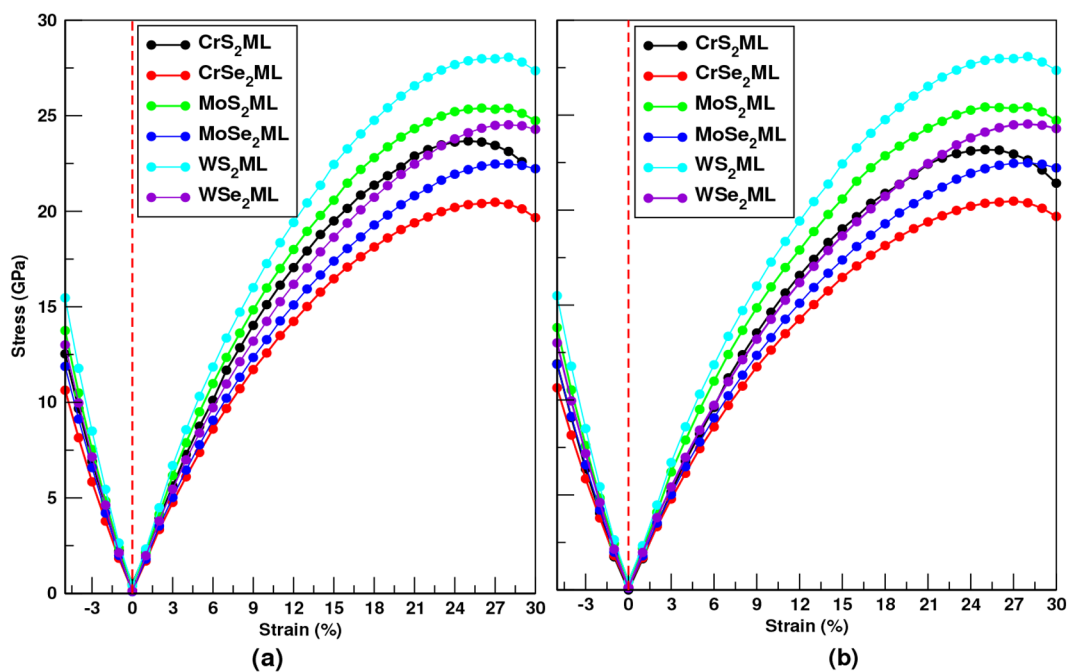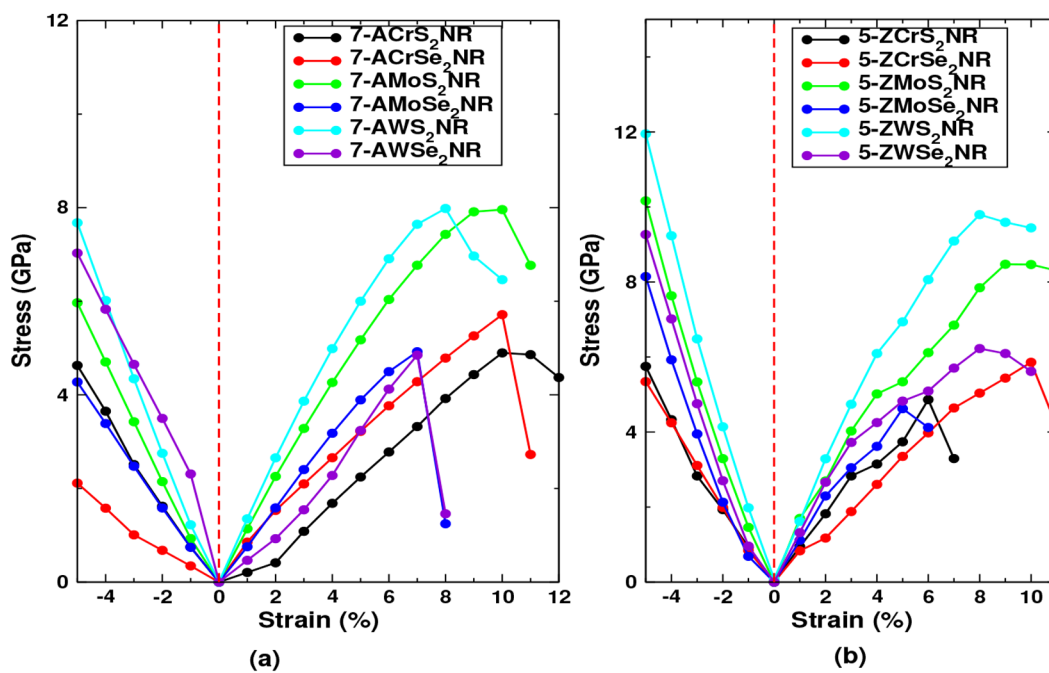
Figure 2. Stress vs strain curves for MX_2MLs. Red vertical line at $\epsilon = 0\%$ corresponds to the optimized structure before strain; $\epsilon < 0$ is CUS and $\epsilon > 0$ is EUS. (a) Uniaxial strain along the x-direction (ϵ_{xx}) and (b) uniaxial strain along the y-direction (ϵ_{yy}). Tensile strength is the peak value of each curve.

Figure 3. Stress vs strain curves for MX_2NRs. Red vertical line at $\epsilon = 0\%$ corresponds to optimized structure before strain; $\epsilon < 0$ is CUS and $\epsilon > 0$ is EUS. (a) Uniaxial strain (ϵ_{yy}) applied to 7-AMX_2NRs along the y-direction (periodic direction). (b) Uniaxial strain (ϵ_{xx}) applied to 5-ZMX_2NRs along the x-direction (periodic direction).

uniaxial strain are given below in Figure 1. M (Cr, Mo, W) atoms occupy one sublattice of the hexagonal sheet, and X (S, Se) atoms occupy the other. However, due to the chemical ratio of M:X = 1:2, the M atom is sandwiched between two nearby X sublattice layers. By cutting single-layer MX_2 along different directions, we obtain two types of nanoribbons viz. armchair (periodic along y-direction) and zigzag (periodic along x-direction). The studied unstrained armchair and

nanoribbons are referred as 7-AMX_2NR and 5-ZMX_2NR, respectively, where 7 and 5 represent the seven vertical columns of armchairs and five horizontal zigzag rows. The uniaxial tensile strain on 2D MLs is applied in the x-direction (ϵ_{xx}) and y-direction (ϵ_{yy}).

The tensile strain is defined as $\epsilon = (a - a_0)/a_0$, where a_0 and a are the lattice constant of unstrained and strained MLs and nanoribbons, respectively. Hence, positive and negative values
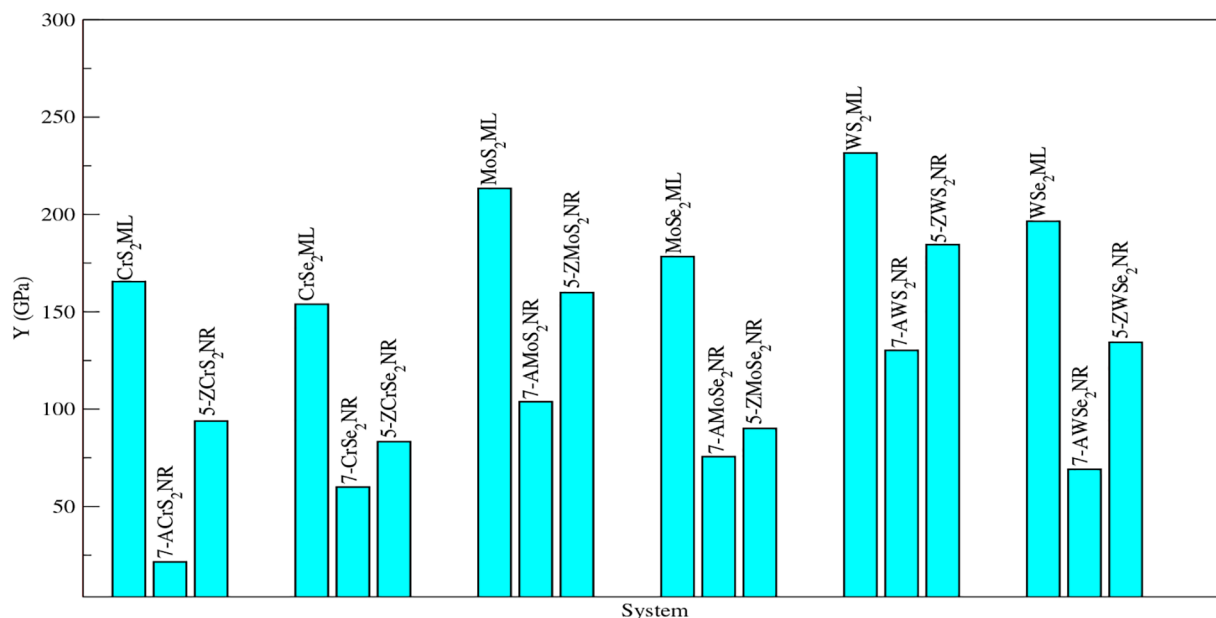
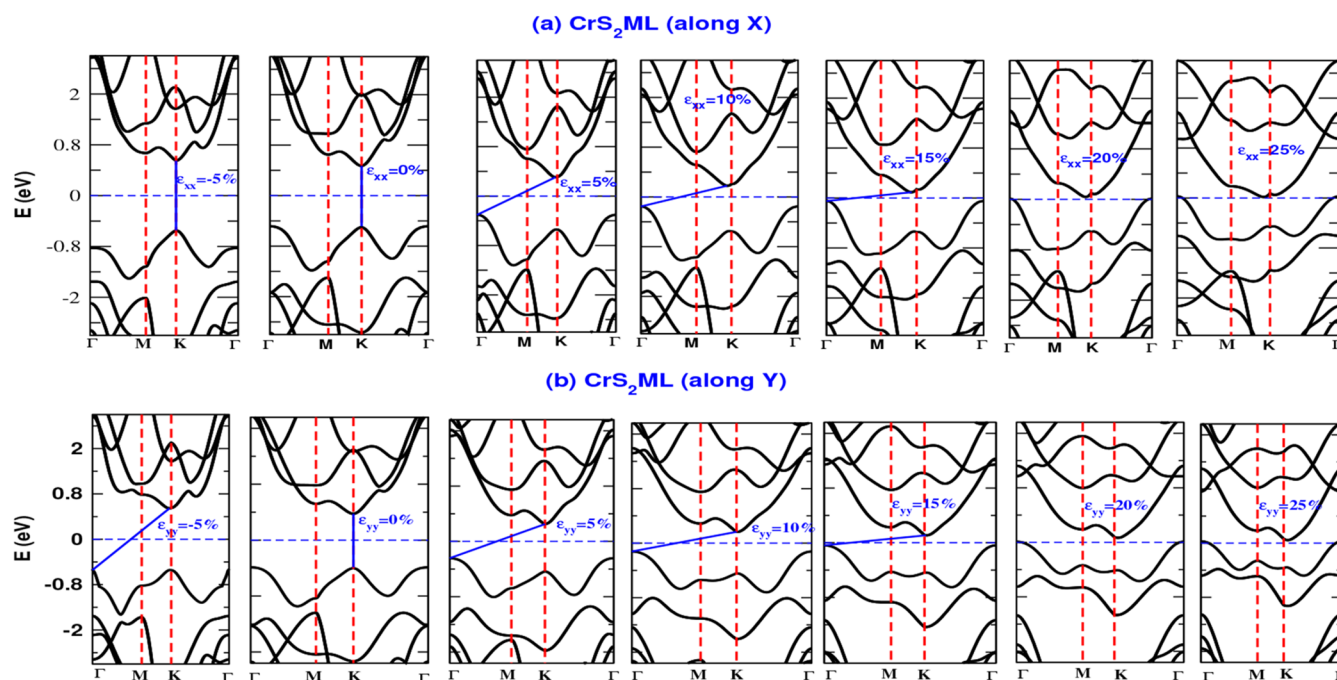**Figure 4.** Young's modulus bar graph for all monolayers and nanoribbons.

Figure 5. Computed isotropic electronic band structures of CrS_2 monolayer along the (a) x-direction with strain $\epsilon_{xx} = -5\%$ to $+25\%$ and (b) y-direction with strain $\epsilon_{yy} = -5\%$ to $+25\%$. Blue color represents the direct or indirect band gap with applied isotropic strain.

of ϵ represent the elongative strain and compressive strain, respectively. In our work, uniaxial strain is applied along the periodic direction to each system of MLs and NRs as shown in Figure 1a−c. The compression and elongation *i.e., both negative and positive uniaxial strain*, range is different for MLs and NRs. For MLs and NRs applied strain ranges from −5 to +30% and −5 to +12%, respectively, as shown in Figures 2 and 3.

The tensile strength of a material represents its capacity to withstand load or resist tension before breaking a material. The higher the tensile strength the greater the capacity of a material to withstand tension. The stress varies directly with applied strain up to a particular limit and then starts decreasing. The

region up to which it varies linearly is the elastic region, followed by a plastic region, and ultimately the system deforms. The maximum value of strain up to which plasticity is retained provides us the value of the ultimate tensile strain, and the corresponding stress value gives the ultimate tensile strength (UTS) (or simply tensile strength (σ^m)) of the system.[69,70] We have applied the strain until UTS is not achieved. The UTS along the x- (σ_{xx}^m) and y-direction (σ_{yy}^m) and the corresponding tensile strain (ϵ_{xx} and ϵ_{yy}) for MX_2MLs are listed in Table 1 and also shown in Figure 2. We observed that the values of ϵ_{xx} and ϵ_{yy} are roughly the same for both the x- and y-directions, respectively. This is due to identical environment of atoms
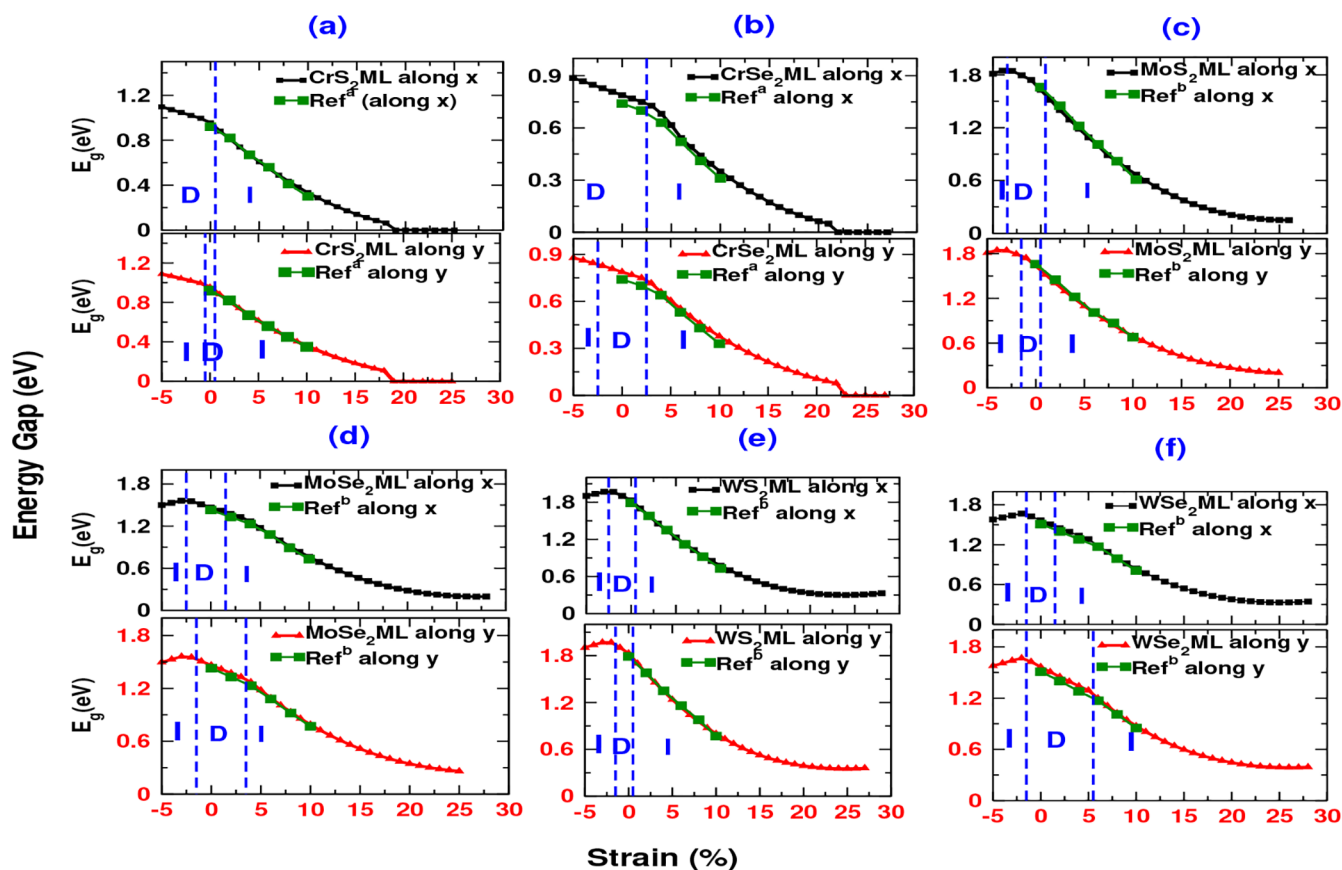
Figure 6. Variation of energy band gap of CrS$_2$ML (a), CrSe$_2$ML (b), MoS$_2$ML (c), MoSe$_2$ML (d), WS$_2$ML (e), and WSe$_2$ML (f) monolayers with CUS and EUS (along the x- and y-direction). For $\epsilon < 0$, the strain is CUS and for $\epsilon > 0$, it is EUS. D and I are the direct and indirect band gaps. (a) Adapted in part from ref 53. Copyright 2014 American Chemical Society. (b) Adapted in part from ref 72. Copyright 2012 American Chemical Society (shown in green).

along both directions in the each MLs. WS$_2$ML has maximum tensile strength and hence this system has most withstand capacity, whereas CrSe$_2$ML has least value. The order of tensile strength for monolayer is WS$_2$ML > MoS$_2$ML > WSe$_2$ML > MoSe$_2$ML > CrS$_2$ML > CrSe$_2$ML.

The armchair and zigzag nanoribbons are deformed at low value as compared to monolayers and have low tensile strength as shown in Figure 3. Among all armchair nanoribbons 7-AWSe$_2$NR has the least tensile strength, whereas 7-AWS$_2$NR has the maximum tensile strength and the order of tensile strength is 7-AWS$_2$NR > 7-AMoS$_2$NR > 7-ACrSe$_2$NR > 7-AMoSe$_2$NR > 7-ACrS$_2$NR > 7-AWSe$_2$NR. On the other hand, among all zigzag nanoribbons 5-ZMoSe$_2$NR shows the least and 5-ZWS$_2$NR shows the maximum tensile strength, and the order of tensile strength in this case is 5-ZWS$_2$NR > 5-ZMoS$_2$NR > 5-ZWSe$_2$NR > 5-ZCrSe$_2$NR > 5-ZCrS$_2$NR > 5-ZMoSe$_2$NR.

We found that WS$_2$ML and their nanoribbons (both armchair and zigzag) have a higher load-withstanding capacity (i.e., highest tensile strength). It is also noted that when the chalcogen atom S changes to Se with the same transition metal, the tensile strength is decreased except for the CrX$_2$ (X = S, Se) nanoribbons.

We have also calculated the Young's modulus (Y) for MX$_2$MLs and MX$_2$NRs. Young's modulus is the slope of stress−strain curve in the elastic region[71] and is given as

$$Y = \frac{\Delta\sigma}{\Delta\epsilon}\bigg|_{\text{elastic region}} \tag{1}$$

The estimated values of Young's modulus for MX$_2$MLs along the x- and y-directions (Y_{xx} and Y_{yy}) and armchair and zigzag nanoribbons are listed in Tables 1 and 2. The observed values of Young's modulus are in good agreement with the previous results. Also the values of Young's modulus along the x- and y-directions are roughly the same. They follow the same trend for the studied MLs as seen for tensile strength because Young's modulus is proportional to tensile strength as stated in eq 1. For armchair and zigzag nanoribbons Young's modulus follows the order 7-AWS$_2$NR > 7-AMoS$_2$NR > 7-AMoSe$_2$NR > 7-AWSe$_2$NR > 7-ACrSe$_2$NR > 7-ACrS$_2$NR and 5-ZWS$_2$NR > 5-ZMoS$_2$NR > 5-ZWSe$_2$NR > 5-ZCrS$_2$NR > 5-ZMoSe$_2$NR > 5-ZCrSe$_2$NR, respectively.

The Young's modulus for each system is shown in Figure 4. It is found that Young's modulus of armchair nanoribbons is lower than the corresponding zigzag nanoribbons, and monolayers have a maximum value of Young's modulus in comparison to all studied nanoribbons. Hence, monolayers are mechanically stronger (WS$_2$ML is max) than the corresponding nanoribbons.

Strain Effect on Electronic Properties of Monolayers. The effects of strain on the electronic band structures of all MX$_2$MLs are shown in Figures 5 and S1−S5. It is noted that the energy band gap (E_g) changes greatly at different strain
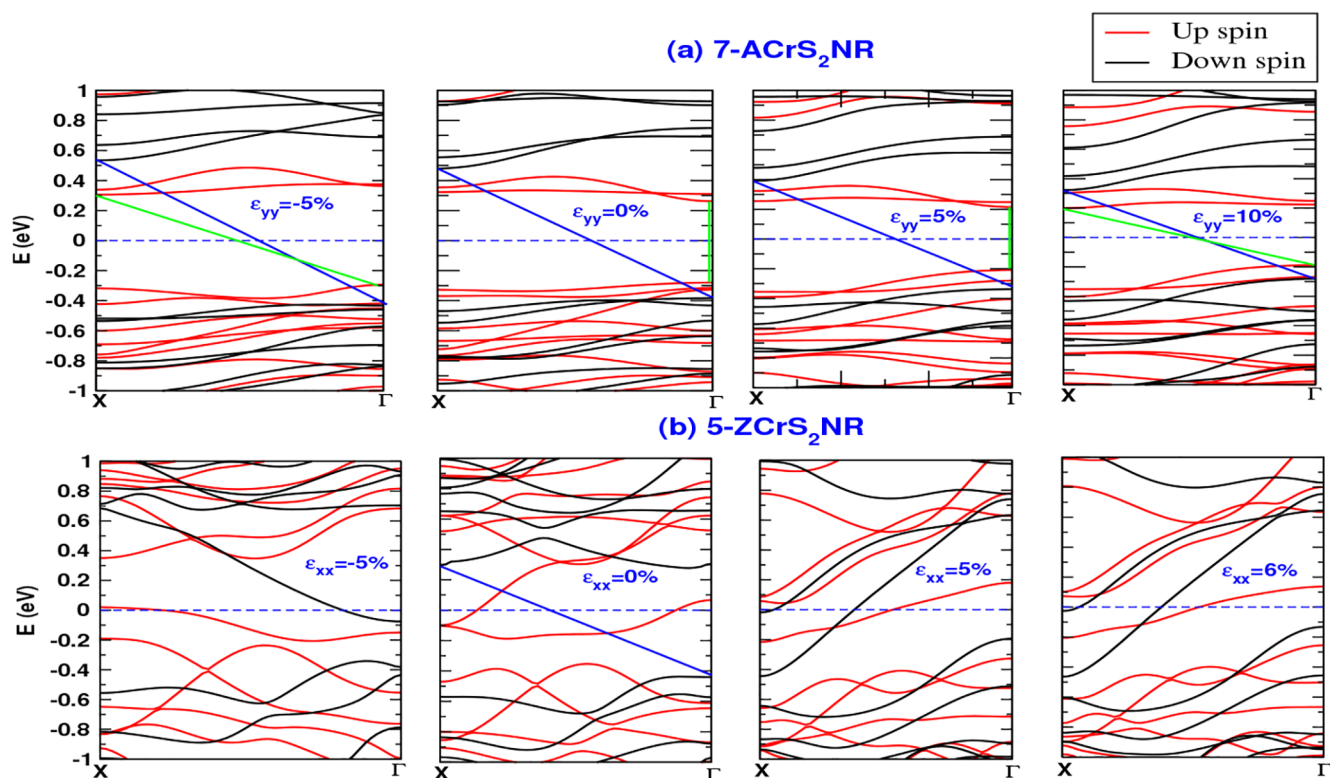
Figure 7. Electronic band structures of CrS$_2$NRs: (a) armchair-nanoribbon along the y-direction with strain ϵ_{yy} = −5% to +10% and (b) zigzag-nanoribbon along the x-direction with strain ϵ_{xx} = −5% to +6%. Green and blue colors represent the direct or indirect band gap corresponding to spin up and spin down, respectively, with applied strain.

percentages, and this variation of energy band gap (E_g) with external applied strain on MLs is shown in Figure 6. The energy band gap reduces with the applied strain along both the x- and y-directions. It switches from a direct (D) to indirect (I) band gap with EUS, and in CUS it switches to an indirect band gap except for CrS$_2$ML and CrSe$_2$ML.

MoX$_2$ML and WX$_2$ML. The energy band gap of MoS$_2$ML along the x- and y-directions increases up to −4% when compression is applied, *i.e.*, $\epsilon < 0$, and after −4% of compression, it decreases as shown in Figure 6(c). A similar trend has been observed for MoSe$_2$ML, WS$_2$ML, and WSe$_2$ML at −3%, −3%, and −2%, respectively (Figure 6(d)−(f)). When strain is positive, *i.e.*, $\epsilon > 0$ for EUS, the band gap of all the monolayers of MoX$_2$ML and WX$_2$ML decreases. The band gap of WS$_2$ML starts increasing slightly beyond ϵ_{xx} = +25% and ϵ_{yy} = +25%, and in WSe$_2$ML, it increases beyond ϵ_{xx} = +25% and ϵ_{yy} = +27%. We observed that the unstrained MoX$_2$MLs and WX$_2$MLs are direct band gap semiconductors, and changes to indirect band gap semiconductors with compression and elongation strain at different strain percentage are as shown in Figure 6(c−f). Our DFT results of E_g resemble earlier data for MoX$_2$ML and WX$_2$ML[72] where only elongative strain has been applied to monolayers as shown in Figure 6(c−f) in green.

CrX$_2$MLs. The electronic band structure at different strain percentages for CrX$_2$MLs are shown in Figures 5 and S1. The variation of E_g with applied strain (both CUS and EUS) for CrX$_2$MLs is shown in Figure 6(a,b) along the x-direction and y-direction. E_g decreases with the increase in EUS $(\epsilon > 0)$ and increases with CUS $(\epsilon < 0)$.

It is noted that unstrained CrX$_2$MLs are direct band gap semiconductors; with elongation along the x-axis they become indirect band gap semiconductors, but with compression along

the x-axis they remain direct band gap semiconductors. On the other hand, unstrained CrS$_2$ML (with strain along y-axis) is a direct band gap semiconductor and becomes an indirect band gap semiconductor with both tensile and compressive strain (Figure 6(a)), whereas CrSe$_2$ML (with strain along the y-axis) is a direct band gap semiconductor from −2% to +2% strain and in the rest of the region it is an indirect band gap semiconductor. These monolayers also show semiconductor to metal transitions with elongative tensile strain. CrS$_2$ML becomes metallic beyond the tensile strain of +19% (for the x- and y-directions), whereas CrSe$_2$ML is metallic beyond +22% (for strain along the x-direction) and +23% (for strain along the y-direction). The estimated variation of E_g of CrX$_2$MLs with applied strain matches with earlier results[53] as shown in Figure 6(a,b).

Strain Effect on Electronic properties of Armchair and Zigzag Nanoribbons. The calculated spin-resolved electronic band structures of armchair and zigzag nanoribbons are shown in Figure 7 and S6−S10. We observed that all of the unstrained armchair nanoribbons are semiconducting and zigzag nanoribbons are metallic except for 5-ZCrS$_2$NR (metallic for up spin and semiconducting for down spin) which behaves like a half metal.[40] The variation of energy band gap with applied strain for all armchair NRs and 5-ZCrS$_2$NR and 5-ZMoS$_2$NR are shown in Figure 8.

5-ZCrS$_2$NR shows half-metal-like behavior in the strain range −2% to +3%, and beyond this it behaves like a metal for both spin up and spin down (Figure 8(g)). 5-ZMoS$_2$NR also shows half-metal-like character at a tensile strain of +8%−9%, and below +8% it behaves like metal (Figure 8(h)).

7-ACrX$_2$NRs are magnetic semiconductors for both spin up and spin down, while all other armchair nanoribbons are
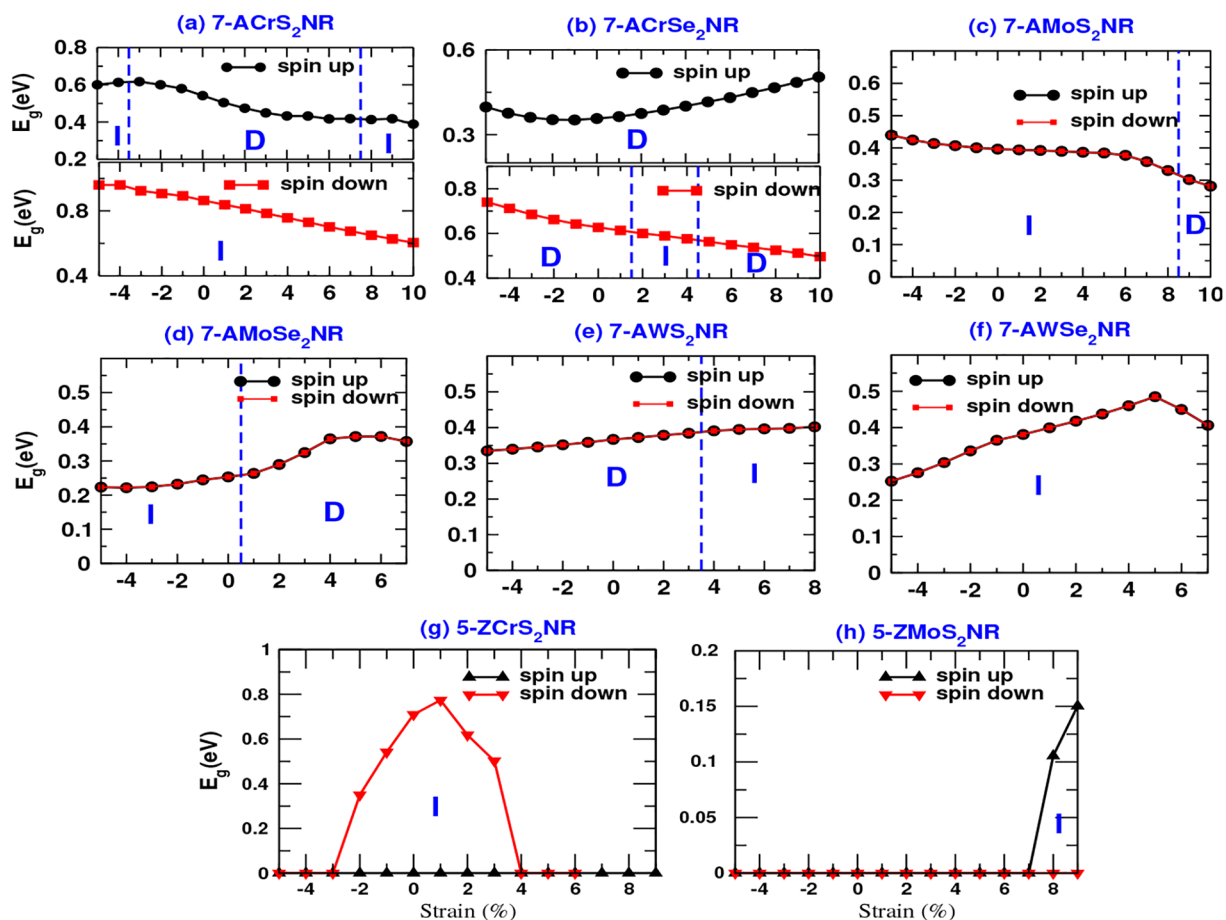
Figure 8. Spin-resolved energy band gap of of 7-ACrS$_2$NR (a), 7-ACrSe$_2$NR (b), 7-AMoS$_2$NR (c), 7-MoSe$_2$NR (d), 7-AWS$_2$NR (e), 7-AWSe$_2$NR (f), 5-ZCrS$_2$NR (g), and 5-ZMoSe$_2$NR (h) with applied strain. The applied strain ranges from −5% to nearly +10%. D and I represent regions (separated by blue dotted vertical lines) of direct to indirect energy band gap at different applied strains.
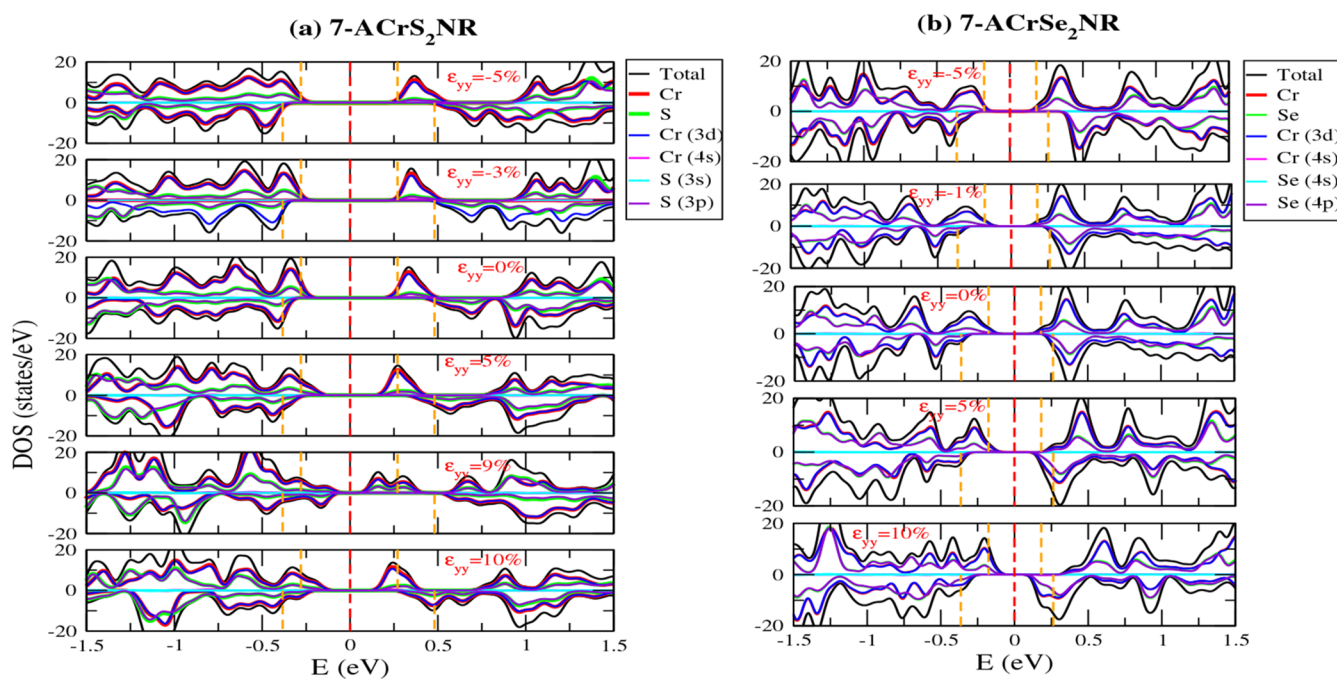

Figure 9. Calculated total density of states (TDOSs) and partial density of states (PDOSs) of armchair nanoribbons 7-ACrS2NR and 7-ACrSe2NR with strain percentage −5% to +10%. Contribution by each atom of Cr, S, and Se for DOS shown by different colors.
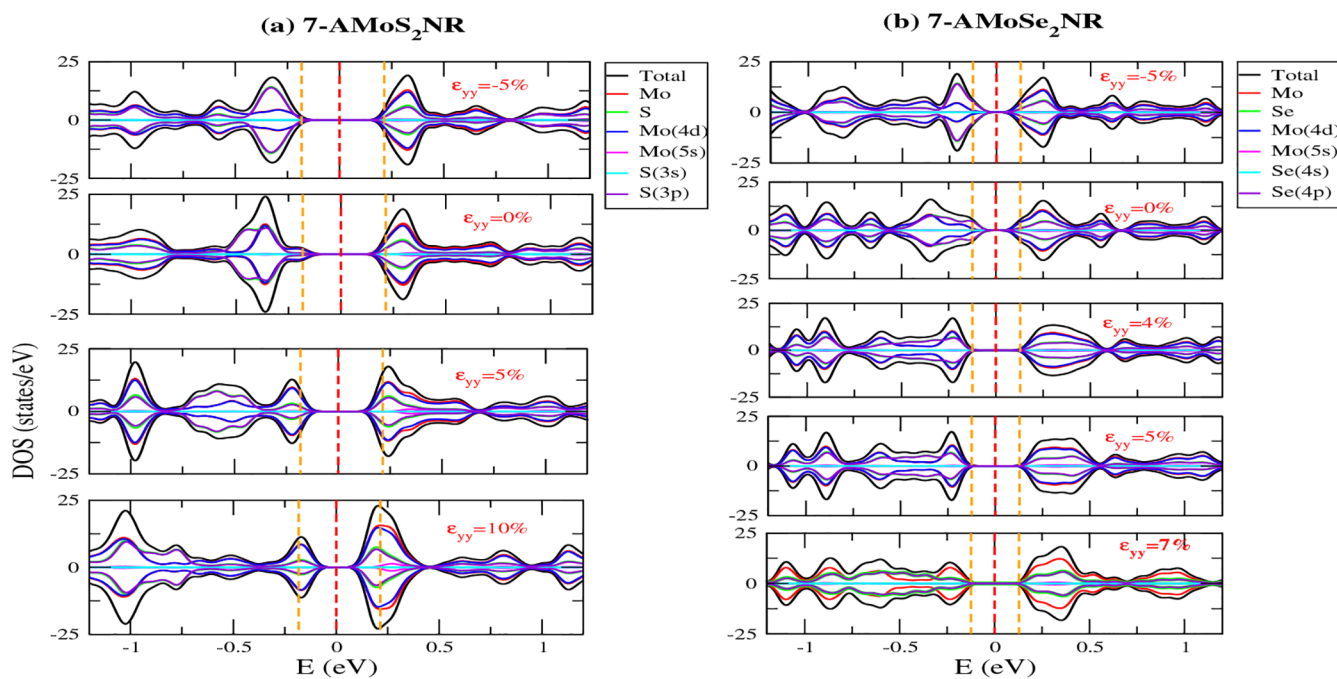
Figure 10. Calculated total density of states (TDOSs) and partial density of states (PDOSs) of armchair nanoribbons 7-AMoS2NR and 7-AMoSe2NR with strain percentage −5% to +10%. Contribution by each atom of Cr, S, and Se for DOS shown by different colors.

nonmagnetic semiconductors as reported earlier in previous work.[40] 7-ACrS$_2$NR for spin up shows indirect−direct−indirect band transitions, while down spin is direct band gap only. Between a strain of −3% to +7% it exists as direct band gap semiconductors and above or 3% strain it exists as indirect band gap semiconductors. In the case of 7-ACrSe$_2$NR, spin down shows direct−indirect−direct band transition at strain of +2% and +4%, and spin up remains a direct band gap semiconductor in the range of compressive and tensile strain.

The nanoribbons 7-AMoX$_2$NR, and 7-AWS$_2$NR have direct-to-indirect or indirect-to-direct band gaps only. 7-AMoS$_2$NR is a direct band gap above the strain of +8% for both spin up and down, while for 7-AMoSe$_2$NR it is direct band gap above (below) +0%, and it is indirect band gap semiconductor (Figure 8(c,d)). These indirect-to-direct band transitions lead us to manufacturing optoelectronics devices. Further 7-AWS$_2$NR is a direct band gap semiconductor below 3%, above that strain it is an indirect band gap semiconductor, and 7-AWSe$_2$NR is an indirect band gap semiconductor for all values of strain (Figure 8(e,f)).

The change in energy band gap with strain (Figure 8) can also be understood from TDOS and PDOS plots which are given in Figures 9, 10, S11, and S12. TDOS and PDOS of 7-ACrS$_2$NR and 7-ACrSe$_2$NR are different for up and down channels, while they are symmetrical for all other armchairs NRs (Figure 9(a,b)). We observed that when the strain is increased from 0% to +10% in 7-AMoS$_2$NR the DOS of valence bands and conduction bands comes closer to the Fermi level in which the Mo atom with 4d and 5s orbitals contributes most as compared to the S atom, while for negative strain (i.e., CUS) the bands do not get far from each other at ϵ_{yy} = −5% (Figure 10(a)). The band gap opening is opposite in 7-AMoSe$_2$NR, where at ϵ_{yy} = −5% bands comes closer and for positive strain (i.e., EUS) at ϵ_{yy} = +4% to ϵ_{yy} = +7%, they move farther away (Figure 10(b)).

The shift in bands in the case of 7-ACrX$_2$NR is different for up and down channels (Figure 9(a,b)). In the positive strain of 7-ACrS$_2$NR, the DOS of conduction bands comes closer to the Fermi level faster than the DOS of valence bands.

Deformation Potential Δ_p. Deformation potential in the linear regime is defined as

$$\Delta_p = \frac{\Delta E_g}{\Delta \epsilon_{xx(yy)}} \tag{2}$$

We have estimated the Δ_p from the E_g vs $\epsilon_{xx}(yy)$ plots in the linear regime near the equilibrium position (ϵ < 2%). The estimated values of Δ_p for the studied monolayers and nanoribbons are listed in Tables 1 and 2. It is calculated for those systems which are semiconductors in nature.

We observed that the Δ_p is higher when the monolayers contain an S atom as compared to an Se atoms in which WS$_2$ML has the highest value at −12.9 eV and CrSe$_2$ML has the least value (−1.9 eV). Our DFT results of MoS$_2$ML and MoSe$_2$ML give almost the same value (−4.5, −11.4 eV) as reported earlier by Kumar et al.[67] (Table 1). In the case of armchair nanoribbons, the value of Δ_p is less as compared to the monolayer and becomes positive for AMoSe$_2$NR, AWS$_2$NR, and AWSe$_2$NR. A smaller value of Δ_p for the nanoribbons suggests that electronic and optoelectronic properties of nanoribbons do not change with strain and hence their opto-electronic and electronic devices can be fabricated on the substrate.[73]

Magnetic Moment. The variation of magnetic moment μ and conductance G, which is the measurement of the number of band lines crossing the Fermi energy (E_F)[74,75] with applied strain, is shown in Figure 11. The conductance is higher when the strain is positive (elongation) as compared to negative (compression).

The magnetic moments (μ) are also affected by the strain, which is shown in Figure 11. All of the zigzag nanoribbons are
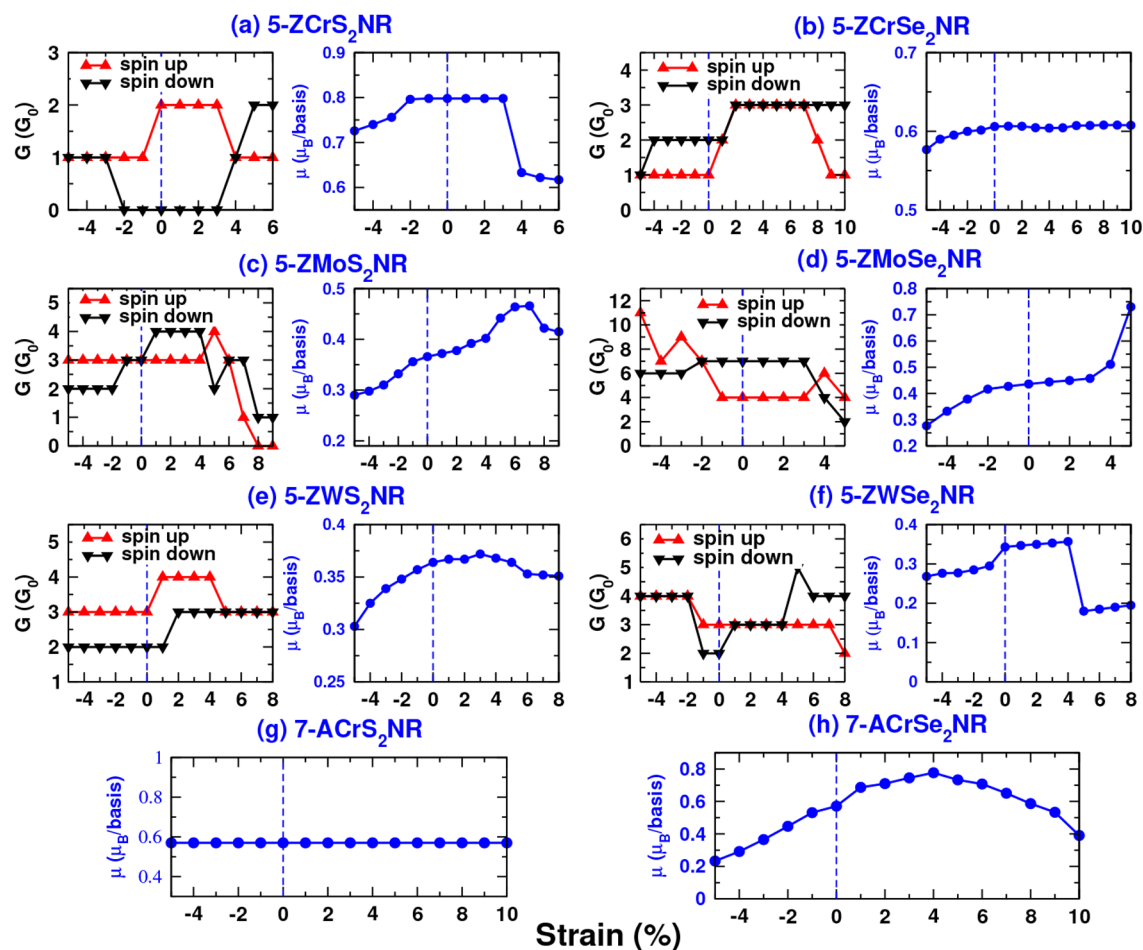
Figure 11. Zigzag nanoribbons MX$_2$ (M = Cr, Mo, W; X = S, Se) (a−f) with applied strain. Conductance (left) and magnetic moment (right side by blue curves) of each zigzag nanoribbon (both spin up and down). Curves (g) and (h) are the armchair nanoribbons which have magnetic moments for the spin up channel.

metallic with some magnetic moment to each value of applied strain. The magnetic moment to each system is mainly attributed by the spin vectors of M = Cr, Mo, W, S or Se atoms at their different positions. The vector representations that contribute to the magnetic moments with applied strain (positive and negative) are shown in Figure 12.

We observed that at 0% strain each system has some value of μ, and as the strain increases to positive direction (elongation) the value also increases and at high positive strain it decreases. In zigzag nanoribbon 5-ZCrS$_2$NR at 0%, μ is 0.8 ($\mu_{B/basis}$), and with compression, its value decreases to 0.73 ($\mu_{B/basis}$) at −5% strain (Figures 11(a) and 12 (a)), but when the strain is positive (elongation), it is almost constant and then decreases to 0.61 ($\mu_{B/basis}$) at +4%.

This is due to the magnitude of spin vectors contribution by Cr atoms only at the left and right edges (Figure 12(a)). In compression, the magnitude of spin vectors decreases which results in a decrease in the value of μ. Hence, the magnetic moment is proportional to the magnitude of the spin vectors of each atom (Figure 12). Similarly, we can see this trend in 5-ZCrSe$_2$NR, where each Cr-atom contributes to the magnetic moment at different percentages of strain (−5%, 0%, +5%, +10%).

Contributions by S and Se atoms are also observed in the case of ZMoX$_2$ and ZWX$_2$ along with transition-metal atoms

(M = Mo, W), and the magnitude of Mo spin vectors is high in 5-ZMoSe$_2$NR, which continues increasing with positive strain.

Two armchair nanoribbons have magnetic moment only for spin up channels, as shown in Figures 11(g,h) and 12 (g,h). Also we found that the CrX$_2$ systems show magnetic moments only due to the Cr atoms. Thus, these spin based materials can be useful for spintronics devices.

■ CONCLUSION

In summary, we performed first-principle calculations to study the electronic and mechanical properties of various transition-metal dichalcogenides TMDs MX$_2$ (where M = Cr, Mo, W and X = S, Se) in their two-dimensional and one-dimensional structures under different strain percentages using DFT theory. We have used uniaxial compressive- and elongation-type strains to each systems. We found that each monolayer and nanoribbon is stretchable up to a particular strain percentage and also the effect of strain is least in monolayers as compared to nanoribbons. The high value of tensile strength and Young's modulus in monolayers reveals to us that they have greater capacity to withstand tension. In electronic properties, the band gap decreases with positive strain (EUS) and increases up to −4% in negative strain (CUS) and all the unstrained nonmagnetic monolayers and armchair nanoribbons are direct band gap semiconductors, and by applying strain, they are
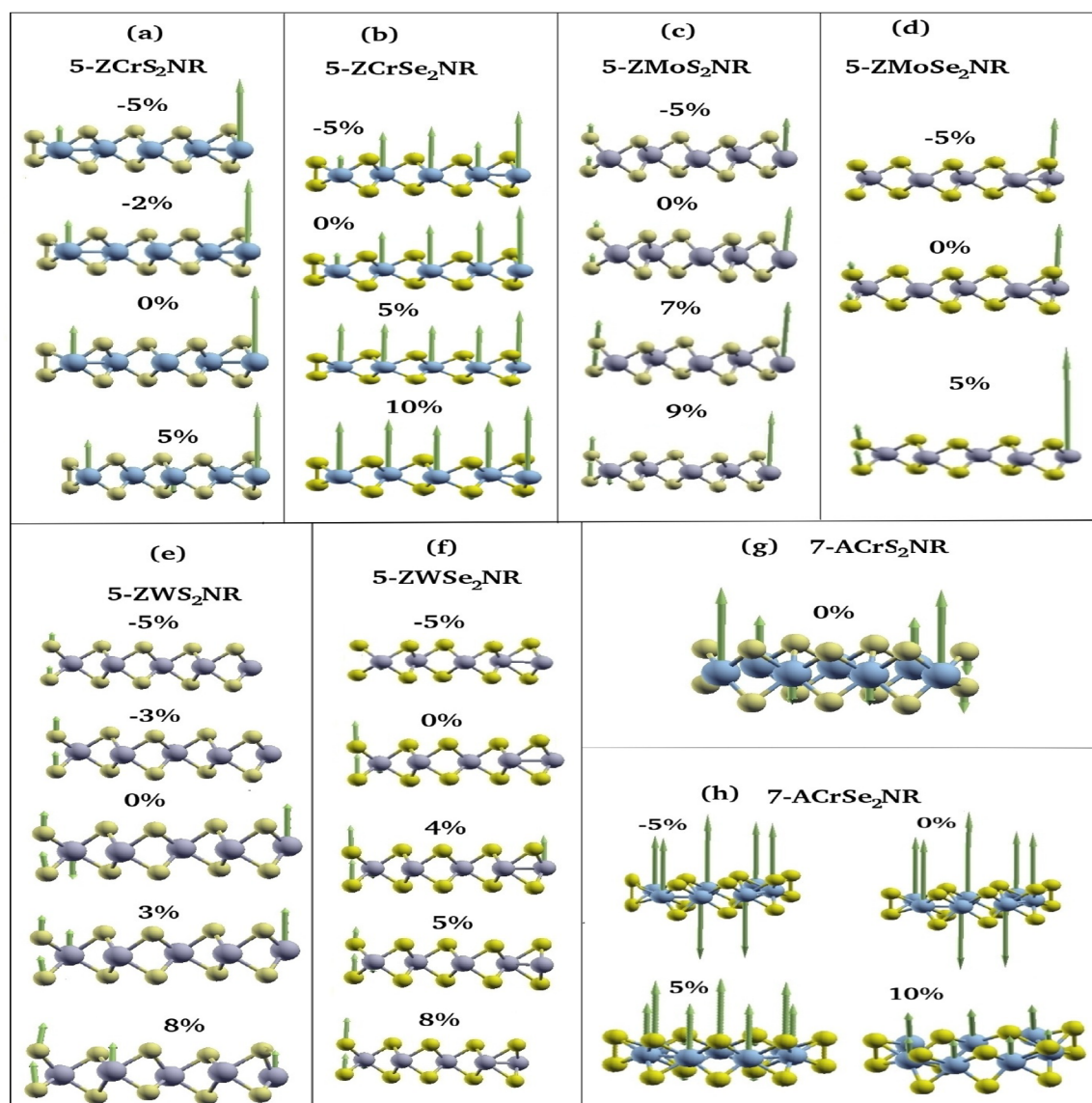
Figure 12. Spin vector representations of zigzag nanoribbons MX_2 (M = Cr, Mo, W; X = S, Se) with strain. Structure (g) and (h) are for armchair nanoribbons with some value of magnetic moment for the spin up channel.

changed from direct to indirect and vice versa. All metallic zigzag nanoribbons (ZMX_2) and spin up channels of 7-CrS_2NR and 7-$CrSe_2NR$ are also affected by strain. Ferromagnetic states of metallic zigzag nanoribbons including spin up channels of 7-CrS_2NR and 7-$CrSe_2NR$ show half-metal-like behavior in different strain ranges. The magnetic moment increases with strain, and with further increases in strain its value decreases for different systems. This effect is mainly caused by transition-metal atoms (M = Cr, Mo, W). Thus, our studies suggest that the strain engineering in the TMD monolayers and nanoribbons have diverse applications in nanodevices such as FETs, optoelectronics, spintronics, and photovoltaic cells.

ASSOCIATED CONTENT

Supporting Information

The Supporting Information is available free of charge at https://pubs.acs.org/doi/10.1021/acsomega.2c04763.

Electronic band gap variations with applied strain in CrS_2, $CrSe_2$, MoS_2, $MoSe_2$, WS_2, and WSe_2 monolayers along the x-direction and y-direction. Armchair and zigzag nanoribbons are periodic along the y- and x-direction; hence, strain is also in one direction. It also contains the density of states (DOS) and partial density of states (PDOS) contributions in monolayer (2D) and nanoribbon (1D) systems (PDF)

AUTHOR INFORMATION

Corresponding Author

Anjna Devi − *Himachal Pradesh University, Shimla 171005, India; Department of Physics, Swami Vivekanand Government College, Ghumarwin, Himachal Pradesh 174021, India;* ⊙ orcid.org/0000-0002-9336-2240; Email: anjnahpu90@gmail.com

Authors

Narender Kumar − *Department of Physics, College of Science, United Arab Emirates University, 15551 Al Ain, UAE*

Abu Thakur − *Department of Physics, Swami Vivekanand Government College, Ghumarwin, Himachal Pradesh 174021, India*

Arun Kumar − *Department of Physics, Swami Vivekanand Government College, Ghumarwin, Himachal Pradesh 174021, India*

Amarjeet Singh − *Himachal Pradesh University, Shimla 171005, India*

P. Kumar Ahluwalia − *Himachal Pradesh University, Shimla 171005, India*

Complete contact information is available at:
https://pubs.acs.org/10.1021/acsomega.2c04763

Notes

The authors declare no competing financial interest.

■ REFERENCES

(1) Zhang, R.; Cheung, R. In *Two-Dimensional Materials*; Nayak, P. K., Ed.; INTECH open science open minds, 2016; Chapter 10, pp 219−246.

(2) Cheng, J.; Wang, C.; Zou, X.; Liao, L. Recent advances in optoelectronic devices based on 2D materials and their heterostructures. *Advanced Optical Materials* 2019, 7, 1800441.

(3) Lan, C.; Shi, Z.; Cao, R.; Li, C.; Zhang, H. 2D materials beyond graphene toward Si integrated infrared optoelectronic devices. *Nanoscale* 2020, 12, 11784−11807.

(4) Zhang, M.; Wu, Q.; Zhang, F.; Chen, L.; Jin, X.; Hu, Y.; Zheng, Z.; Zhang, H. 2D black phosphorus saturable absorbers for ultrafast photonics. *Advanced Optical Materials* 2019, 7, 1800224.

(5) He, J.; Tao, L.; Zhang, H.; Zhou, B.; Li, J. Emerging 2D materials beyond graphene for ultrashort pulse generation in fiber lasers. *Nanoscale* 2019, 11, 2577−2593.

(6) Devi, A.; Kumar, A.; Singh, A.; Ahluwalia, P. K. A comparative spin dependent first principle study of monolayer (2D), armchair and zigzag nanoribbon (1D) of chromium disulfide (CrS2). *AIP Conf. Proc.* 2020, 2265, 030701.

(7) Devi, A.; Kumar, A.; Singh, A.; Ahulwalia, P. K. A comparative study on phonon spectrum and thermal properties of graphene, silicene and phosphorene. *AIP Conf. Proc.* 2019, 2115, 030386.

(8) Cui, C.; Xue, F.; Hu, W.-J.; Li, L.-J. Two-dimensional materials with piezoelectric and ferroelectric functionalities. *npj 2D Materials and Applications* 2018, 2, 1−14.

(9) Glavin, N. R.; Muratore, C.; Snure, M. Toward 2D materials for flexible electronics: opportunities and outlook. *Oxford Open Materials Science* 2020, 1, 1−7.

(10) Jiang, H.; Zheng, L.; Liu, Z.; Wang, X. Two-dimensional materials: From mechanical properties to flexible mechanical sensors. *InfoMat* 2020, 2, 1077−1094.

(11) Manzeli, S.; Dumcenco, D.; Migliato Marega, G.; Kis, A. Self-sensing, tunable monolayer MoS2 nanoelectromechanical resonators. *Nat. Commun.* 2019, 10, 1−7.

(12) Novoselov, K. S.; Geim, A. K.; Morozov, S. V.; Jiang, D.; Zhang, Y.; Dubonos, S. V.; Grigorieva, I. V.; Firsov, A. A. Electric field effect in atomically thin carbon films. *science* 2004, 306, 666−669.

(13) Novoselov, K. S.; Geim, A. K.; Morozov, S. V.; Jiang, D.; Katsnelson, M. I.; Grigorieva, I.; Dubonos, S.; Firsov, A. A. Two-dimensional gas of massless Dirac fermions in graphene. *nature* 2005, 438, 197−200.

(14) Novoselov, K. S.; Geim, A. The rise of graphene. *Nat. Mater.* 2007, 6, 183−191.

(15) Bolotin, K. I.; Sikes, K. J.; Jiang, Z.; Klima, M.; Fudenberg, G.; Hone, J. e.; Kim, P.; Stormer, H. Ultrahigh electron mobility in suspended graphene. *Solid state communications* 2008, 146, 351−355.

(16) Balandin, A. A.; Ghosh, S.; Bao, W.; Calizo, I.; Teweldebrhan, D.; Miao, F.; Lau, C. N. Superior thermal conductivity of single-layer graphene. *Nano Lett.* 2008, 8, 902−907.

(17) Zhou, Y.; Bao, Q.; Varghese, B.; Tang, L. A. L.; Tan, C. K.; Sow, C.-H.; Loh, K. P. Microstructuring of graphene oxide nanosheets using direct laser writing. *Adv. Mater.* 2010, 22, 67−71.

(18) Castro Neto, A. H.; Guinea, F.; Peres, N. M. R.; Novoselov, K. S.; Geim, A. K. The electronic properties of graphene. *Reviews of modern physics* 2009, 81, 109.

(19) Ando, T. Theory of electronic states and transport in carbon nanotubes. *J. Phys. Soc. Jpn.* 2005, 74, 777−817.

(20) Ando, T. Physics of GrapheneZero-Mode Anomalies and Roles of Symmetry. *Prog. Theor. Phys. Suppl.* 2008, 176, 203−226.

(21) Pakdel, A.; Zhi, C.; Bando, Y.; Golberg, D. Low-dimensional boron nitride nanomaterials. *Mater. Today* 2012, 15, 256−265.

(22) Ni, Z.; Liu, Q.; Tang, K.; Zheng, J.; Zhou, J.; Qin, R.; Gao, Z.; Yu, D.; Lu, J. Tunable bandgap in silicene and germanene. *Nano Lett.* 2012, 12, 113−118.

(23) Houssa, M.; Scalise, E.; Sankaran, K.; Pourtois, G.; Afanas' Ev, V.; Stesmans, A. Electronic properties of hydrogenated silicene and germanene. *Appl. Phys. Lett.* 2011, 98, 223107.

(24) Mahatha, S.; Patel, K.; Menon, K. S. Electronic structure investigation of MoS2 and MoSe2 using angle-resolved photoemission spectroscopy and ab initio band structure studies. *J. Phys.: Condens. Matter* 2012, 24, 475504.

(25) Radisavljevic, B.; Radenovic, A.; Brivio, J.; Giacometti, V.; Kis, A. Single-layer MoS 2 transistors. *Nature Nanotechnol.* 2011, 6, 147−150.

(26) Kar, M.; Sarkar, R.; Pal, S.; Sarkar, P. Engineering the magnetic properties of PtSe2 monolayer through transition metal doping. *J. Phys.: Condens. Matter* 2019, 31, 145502.

(27) Fan, X.-L.; An, Y.-R.; Guo, W.-J. Ferromagnetism in transitional metal-doped MoS 2 monolayer. *Nanoscale Res. Lett.* 2016, 11, 1−10.

(28) Guo, C.; Xia, C.; Fang, L.; Wang, T.; Liu, Y. Tuning anisotropic electronic transport properties of phosphorene via substitutional doping. *Phys. Chem. Chem. Phys.* 2016, 18, 25869−25878.

(29) Anasori, B.; Lukatskaya, M. R.; Gogotsi, Y. 2D metal carbides and nitrides (MXenes) for energy storage. *Nature Reviews Materials* 2017, 2, 1−17.

(30) Tang, X.; Guo, X.; Wu, W.; Wang, G. 2D metal carbides and nitrides (MXenes) as high-performance electrode materials for lithium-based batteries. *Adv. Energy Mater.* 2018, 8, 1801897.

(31) Dankert, A.; Langouche, L.; Kamalakar, M. V.; Dash, S. P. High-performance molybdenum disulfide field-effect transistors with spin tunnel contacts. *ACS Nano* 2014, 8, 476−482.

(32) Singh, E.; Singh, P.; Kim, K. S.; Yeom, G. Y.; Nalwa, H. S. Flexible molybdenum disulfide (MoS2) atomic layers for wearable electronics and optoelectronics. *ACS Appl. Mater. Interfaces* 2019, 11, 11061−11105.

(33) Wang, Q. H.; Kalantar-Zadeh, K.; Kis, A.; Coleman, J. N.; Strano, M. S. Electronics and optoelectronics of two-dimensional transition metal dichalcogenides. *Nature Nanotechnol.* 2012, 7, 699−712.

(34) Mak, K. F.; Lee, C.; Hone, J.; Shan, J.; Heinz, T. F. Atomically Thin MoS$_2$: A New Direct-Gap Semiconductor. *Phys. Rev. Lett.* 2010, 105, 1−4.

(35) Koppens, F. H. L.; Mueller, T.; Avouris, P.; Ferrari, A. C.; Vitiello, M. S.; Polini, M. Photodetectors based on graphene, other two-dimensional materials and hybrid systems. *Nat. Nanotechnol.* 2014, 9, 780−793.

(36) Ponraj, J. S.; Xu, Z.; Dhanabalan, S. C.; Mu, H.; Wang, Y.; Yuan, J.; Li, P.; Thakur, S.; Ashrafi, M.; Mccoubrey, K. Photonics and optoelectronics of two-dimensional materials beyond graphene. *Nanotechnology* 2016, 27, 462001.

(37) Ping, J.; Fan, Z.; Sindoro, M.; Ying, Y.; Zhang, H. Recent advances in sensing applications of two-dimensional transition metal

dichalcogenide nanosheets and their composites. *Adv. Funct. Mater.* **2017**, *27*, 1605817.

(38) Zhang, G.; Zhang, Y.-W. Thermoelectric properties of two-dimensional transition metal dichalcogenides. *J. Mater. Chem. C* **2017**, *5*, 7684−7698.

(39) Chhowalla, M.; Shin, H. S.; Eda, G.; Li, L.-J.; Loh, K. P.; Zhang, H. The chemistry of two-dimensional layered transition metal dichalcogenide nanosheets. *Nature Chem.* **2013**, *5*, 263−275.

(40) Devi, A.; Kumar, A.; Ahluwalia, P.; Singh, A. Novel properties of transition metal dichalcogenides monolayers and nanoribbons (MX2, where M = Cr, Mo, W and X = S, Se): A spin resolved study. *Materials Science and Engineering: B* **2021**, *271*, 115237.

(41) Zhang, X.; Teng, S. Y.; Loy, A. C. M.; How, B. S.; Leong, W. D.; Tao, X. Transition metal dichalcogenides for the application of pollution reduction: A review. *Nanomaterials* **2020**, *10*, 1012.

(42) Xia, Y.; Yang, P.; Sun, Y.; Wu, Y.; Mayers, B.; Gates, B.; Yin, Y.; Kim, F.; Yan, H. One-dimensional nanostructures: synthesis, characterization, and applications. *Advanced materials* **2003**, *15*, 353−389.

(43) Wang, X.; Li, Y. Solution-based synthetic strategies for 1-D nanostructures. *Inorg. Chem.* **2006**, *45*, 7522−7534.

(44) Devi, A.; Kumar, A.; Kumar, T.; Bharti; Adhikari, R.; Ahluwalia, P.; Singh, A. Structural, electronic and magnetic properties of CrmSn and CrmSen nanoflakes: An ab initio investigation. *Physica E: Low-dimensional Systems and Nanostructures* **2021**, *134*, 114825.

(45) Davelou, D.; Kopidakis, G.; Kioseoglou, G.; Remediakis, I. N. MoS2 nanostructures: Semiconductors with metallic edges. *Solid state communications* **2014**, *192*, 42−46.

(46) Li, B. L.; Wang, J.; Zou, H. L.; Garaj, S.; Lim, C. T.; Xie, J.; Li, N. B.; Leong, D. T. Low-dimensional transition metal dichalcogenide nanostructures based sensors. *Adv. Funct. Mater.* **2016**, *26*, 7034−7056.

(47) Xu, H.; Ding, Z.; Nai, C. T.; Bao, Y.; Cheng, F.; Tan, S. J.; Loh, K. P. Controllable synthesis of 2D and 1D MoS2 nanostructures on Au surface. *Adv. Funct. Mater.* **2017**, *27*, 1603887.

(48) Autere, A.; Jussila, H.; Marini, A.; Saavedra, J.; Dai, Y.; Säynätjoki, A.; Karvonen, L.; Yang, H.; Amirsolaimani, B.; Norwood, R. A.; et al. Optical harmonic generation in monolayer group-VI transition metal dichalcogenides. *Phys. Rev. B* **2018**, *98*, 115426.

(49) Komsa, H.-P.; Kotakoski, J.; Kurasch, S.; Lehtinen, O.; Kaiser, U.; Krasheninnikov, A. V. Two-dimensional transition metal dichalcogenides under electron irradiation: defect production and doping. *Physical review letters* **2012**, *109*, 035503.

(50) Gao, Y.-P.; Wu, X.; Huang, K.-J.; Xing, L.-L.; Zhang, Y.-Y.; Liu, L. Two-dimensional transition metal diseleniums for energy storage application: a review of recent developments. *CrystEngComm* **2017**, *19*, 404−418.

(51) Qi, Z.; Cao, P.; Park, H. S. Density functional theory calculation of edge stresses in monolayer MoS2. *J. Appl. Phys.* **2013**, *114*, 163508.

(52) Zhang, Z.; Wang, J.; Song, C.; Mao, H.; Zhao, Q. Tuning band gaps of transition metal dichalcogenides WX2 (X= S, Se) nanoribbons by external strain. *J. Nanosci. Nanotechnol.* **2016**, *16*, 8090−8095.

(53) Guo, H.; Lu, N.; Wang, L.; Wu, X.; Zeng, X. C. Tuning electronic and magnetic properties of early transition-metal dichalcogenides via tensile strain. *J. Phys. Chem. C* **2014**, *118*, 7242−7249.

(54) Carrascoso, F.; Li, H.; Frisenda, R.; Castellanos-Gomez, A. Strain engineering in single-, bi-and tri-layer MoS 2, MoSe 2, WS 2 and WSe 2. *Nano Research* **2021**, *14*, 1−6.

(55) Pan, H.; Zhang, Y.-W. Tuning the electronic and magnetic properties of MoS2 nanoribbons by strain engineering. *J. Phys. Chem. C* **2012**, *116*, 11752−11757.

(56) Zhang, H.; Li, X.-B.; Liu, L.-M. Tunable electronic and magnetic properties of WS2 nanoribbons. *J. Appl. Phys.* **2013**, *114*, 093710.

(57) Ordejón, P.; Artacho, E.; Soler, J. M. Self-consistent order-N density-functional calculations for very large systems. *Phys. Rev. B* **1996**, *53*, R10441.

(58) Soler, J. M.; Artacho, E.; Gale, J. D.; García, A.; Junquera, J.; Ordejón, P.; Sánchez-Portal, D. The SIESTA method for ab initio order-N materials simulation. *J. Phys.: Condens. Matter* **2002**, *14*, 2745.

(59) Perdew, J. P.; Ruzsinszky, A.; Csonka, G. I.; Vydrov, O. A.; Scuseria, G. E.; Constantin, L. A.; Zhou, X.; Burke, K. Restoring the density-gradient expansion for exchange in solids and surfaces. *Physical review letters* **2008**, *100*, 136406.

(60) Monkhorst, H. J.; Pack, J. D. Special points for Brillouin-zone integrations. *Phys. Rev. B* **1976**, *13*, 5188.

(61) Ding, Y.; Wang, Y.; Ni, J.; Shi, L.; Shi, S.; Tang, W. First principles study of structural, vibrational and electronic properties of graphene-like MX2 (M= Mo, Nb, W, Ta; X= S, Se, Te) monolayers. *Physica B: Condensed Matter* **2011**, *406*, 2254−2260.

(62) Tian, X.-H.; Zhang, J.-M. The electronic, magnetic and optical properties of single-layer CrS2 with vacancy defects. *J. Magn. Magn. Mater.* **2019**, *487*, 165300.

(63) Kumar, A.; Mohan, B.; Kumar, A.; Ahluwalia, P. K. Mechanically strained tuning of the electronic and dielectric properties of monolayer honeycomb structure of tungsten disulphide-(WS2). *AIP Conf. Proc.* **2013**, *1512*, 1242−1243.

(64) Bertolazzi, S.; Brivio, J.; Kis, A. Stretching and Breaking of Ultrathin MoS2. *ACS Nano* **2011**, *5*, 9703−9709.

(65) Deng, S.; Li, L.; Li, M. Stability of direct band gap under mechanical strains for monolayer MoS2, MoSe2, WS2 and WSe2. *Physica E: Low-dimensional Systems and Nanostructures* **2018**, *101*, 44−49.

(66) Hung, N. T.; Nugraha, A. R. T.; Saito, R. Two-dimensional MoS$_2$ electromechanical actuators. *Journal of Physics D Applied Physics* **2018**, *51*, 075306.

(67) Kumar, A.; Ahluwalia, P. Mechanical strain dependent electronic and dielectric properties of two-dimensional honeycomb structures of MoX2 (X = S, Se, Te). *Physica B: Condensed Matter* **2013**, *419*, 66−75.

(68) Cai, Y.; Zhang, G.; Zhang, Y.-W. Polarity-Reversed Robust Carrier Mobility in Monolayer MoS2 Nanoribbons. *J. Am. Chem. Soc.* **2014**, *136*, 6269−6275.

(69) Thakur, S.; Kumar, N.; Kumar, R.; Devi, A.; Kumar, A. Band gap engineering of tungsten disulfide (WS2) nanoribbon by applying elastic strain and electric field. *AIP Conference Proceedings.* **2020**, 030698.

(70) Kapoor, P.; Kumar, J.; Kumar, A.; Kumar, A.; Ahluwalia, P. Electronic, Mechanical, and Dielectric Properties of Two-Dimensional Atomic Layers of Noble Metals. *J. Electron. Mater.* **2017**, *46*, 650−659.

(71) Kittel, C.*Introduction to Solid State Physics*; Wiley, 2004.

(72) Johari, P.; Shenoy, V. B. Tuning the electronic properties of semiconducting transition metal dichalcogenides by applying mechanical strains. *ACS Nano* **2012**, *6*, 5449−5456.

(73) Wiktor, J.; Pasquarello, A. Absolute deformation potentials of two-dimensional materials. *Phys. Rev. B* **2016**, *94*, 245411.

(74) Agrawal, B. K.; Singh, V.; Srivastava, R.; Agrawal, S. Ab initio study of the structural, electronic, and optical properties of ultrathin lead nanowires. *Phys. Rev. B* **2006**, *74*, 245405.

(75) Kumar, A.; Kumar, A.; Ahluwalia, P. Ab initio study of structural, electronic and dielectric properties of free standing ultrathin nanowires of noble metals. *Physica E: Low-dimensional Systems and Nanostructures* **2012**, *46*, 259−269.